Supporting Information

Bergmann et al. 10.1073/pnas.1001569107

SI Text

Synchrotron Rapid Scanning X-ray Fluorescence (XRF). ***Elemental mapping details.*** The readout and control system is based on a combination of custom and home built hardware and software and is described elsewhere (1). The essential feature is that an entire horizontal line of data is read and stored into a local memory area. At the end of each line when the scanning stage moves to the next line the data are transferred to the control computer. This system virtually eliminates any dead time in the scanning. In order to synchronize the readout and image of each line in the bidirectional scans, the readout time per pixel is adjustable to a precision of 10 ns. A lower priority software process transfers the buffered data to the computer, and any delays at the communication link or host computer do not affect the data acquisition timing. In addition to programmable measurement timing and input/output polarity, the electronics can convert data to 16-bit values and send measurement results only from specified counters to reduce the amount of transferred data.

Because some XRF lines are close to or overlap those of neighboring elements, a map assigned to an element might have some residual contributions from other elements. This was not a problem for the well known Mn Kβ/Fe Kα overlap (because except for the dendrites Mn signals were typically much smaller than Fe signals) but was a problem in resolving the Ti Kα from the Ba Lα. We suspect that counts in this window which correlate with high Fe are caused by trace Ti in oxyhydroxide precipitates but that bright spots which correlate with P are due to a Ba for Ca substitution in the bone mineral. However concentrations were too low to allow us to resolve these two elements using these or other characteristic emission lines and so we simply report a convolved map for this window.

Point analysis details. Three key measurement challenges confront quantification of point analyses in this case:

1. uncertainty in incident photon flux,
2. high surface relief of the specimen, and
3. depth heterogeneity of the sample.

(1) Incident photon flux was initially measured with an N_2 filled ion chamber and finally adjusted using Ca yield as an internal check.

(2) Surface relief was accounted for by measuring the total relief of the specimen (7.5 mm), integrating the total number of counts accumulated in the detector over the analysis time, and then using the square root of the integrated counts to scale the sample distance relative to the detector in the known relief range, with maximum counts used to set minimum distance and minimum counts used to set maximum distance. Furthest (rachis) and closest (sediment 3) points were assigned maximum and minimum distances and the remaining points interpolated using the equation

$$d_i = d_{\min} + \frac{(c_{\max} - c_i)^{\frac{1}{2}}}{(c_{\max} - c_{\min})^{\frac{1}{2}}} * 7.5 \qquad \textbf{[S1]}$$

where d is distance in millimeters and c is integrated counts.

This correction was small for the high-Z analyses because the topography contributes only a 10% variation in the total sample-detector distance. For the low-Z elements this was a relatively large correction because topography represents as much as a 35% difference in distance. Checks on this calculation were provided by comparing the distance results for the low-Z elements with the high-Z distances at the same point and also by checking the calculated Ca concentrations (as also discussed below). Because Ca is high in both the matrix and the bone it provided a useful internal standard. Both checks were consistent within the 50% error quoted for the low-Z elements. Integrated count rate was used in order to give best counting statistics for the distance calibration and was suitable in this case both because there was little fluctuation in background from point to point and because the characteristic fluorescence is dominated by calcium which is present at high concentrations throughout the matrix and fossil.

(3) Depth heterogeneity has not been accounted for; we simply note that the trace element contents estimated for the *Archaeopteryx*, especially the transition elements, are most likely to be minimum concentrations due to the fact that the points where bone was analyzed are probably not uniform as a function of depth and the interaction volume of the beam therefore may include sedimentary matrix which would dilute the characteristic yield. Calculations assuming multilayer structure show that large errors will only be produced given our analytical geometry if the bone thickness is less than approximately 30 μm (the thickness of a standard petrographic thin section) at the point analyzed. Given that the thickness of bone is in all cases probably well in excess of this, we assume that this is not the primary source of error in our bone analysis. The rachises, however, may be thinner and are also less electronically dense, and so error caused by depth heterogeneity, while important to note as possible for all points analyzed, will be greatest for the soft tissue.

Raw intensity spectra were converted to elemental concentrations using the PyMCA program (2). Resulting concentrations were calculated from fundamental parameters; i.e., we did not force Ca concentrations to equal the theoretical values of apatite or calcite, we fixed all analytical parameters to one set of values for each set of point analyses (one set for the 3.15-keV analyses, another for the 13.5-keV analyses) and then only adjusted sample distance as described above when calculating the concentrations given in Table 1. This allowed us to estimate errors on the results by comparison to the theoretical Ca concentrations. Fig. S4 shows an example of a full energy dispersive spectrometry spectrum with accompanying fit calculated for the skull point analysis taken at 13.5-keV incident energy. The presence of the bone consolidant created an analytical problem for the low atomic weight elements, because a polyvinyl acetate film several microns thick [as would be typical of a layer of a low concentration emulsion as usually applied to conserve bone (3, 4)] would absorb part of the emitted signal and cause one to underestimate the concentration of Si, S, P, and Cl by as much as 50%.

Image Processing for Figures. Adobe Photoshop (5) was used for rapid turnaround of images as well as to ensure the integrity of the interpreted results. The images of *Archaeopteryx* are generated from X-ray spectra stored in each pixel. In order to create an elemental X-ray image, the raw data are converted from ASCII to a 16-bit TIFF grayscale. Software provided by Dr. Keith Knox (6) extracted and converted the data for each element from the raw ASCII data file into individual 16-bit TIFF grayscale files.

For *Archaeopteryx*, the image created is actually a sophisticated graph with each pixel representing elemental response scaled between 0 and 255. Because each pixel is related to the concentration of the individual elements at that point on the specimen, great care is taken in the processing of the image to ensure the preservation of the trace responses that may provide the smallest

details. The "levels" tool of Photoshop is used to adjust the tonal value of the image until the first response line can be seen in the levels histogram. By moving the white point/highlight slider just prior to the first response in the histogram, the tonal value for the image is redistributed between 0 (black) and the new 255 (white) endpoint. The image midtones are then adjusted between the endpoints to view details in the image.

Banding or beam drift is removed by inverting the I_O channel for the corresponding series of scans as a new layer over an elemental image. The inverted I_O layer is eliminated from the elemental image by setting the Photoshop "blending mode" to "multiply" and adjusting the opacity until the banding visible in the image is uniformly removed. The two images are then combined into a drift corrected image. Row offsets are corrected by selecting alternating rows and the "move" tool until all of the rows are in proper alignment.

Each complete elemental image of the *Archaeopteryx* consists of three separate images corrected in this fashion. The three corrected images for individual elements are stitched together to the closest matching pixels. The levels tool is again used to match tonal quality between the 3 layers. The final image is flattened and saved as a new file name. Additional detailed information for all figures is given below.

Fig. 1 was produced by combining a digital optical light photograph with the grayscale TIFF image of the phosphorous data. Contrast and brightness of the X-ray image were readjusted for comparison to the photograph and annotations were added using Adobe Photoshop Elements 7. Fig. S1 was also made from TIFF images with levels readjusted using Photoshop.

In Fig. 2 the detector count data was analyzed using Matlab 2009 (The Mathworks, Natick, MA). For visualization the original 16-bit detector count values were scaled so that the data range from 0 to the 95th percentile was linearly mapped to 0 to 255 allowing the production of an 8-bit grayscale image. The top 5% of the data for any specific channel were produced by a few, high count spikes, and this mapping provided a consistent method to provide good contrast of the lower intensity features. A false color image was produced by applying the scaled Ca counts to the red channel, the scaled Zn counts to the green channel, and the scaled Mn counts to the blue channel of a 24-bit RGB image. The high Z count values in Figs. 2, 4, and 5 and Fig. S3 are from an area that was imaged 4 times with the detector counts summed.

For Fig. 4 the detector count data was analyzed using Matlab 2009 (The Mathworks, Natick, MA). For visualization the original 16-bit detector count values were scaled so that the data range from 0 to the 95th percentile was linearly mapped to 0 to 255 allowing the production of an 8-bit grayscale image. The top 5% of the data for any specific channel were produced by a few, high count spikes, and this mapping provided a consistent method to provide good contrast of the lower intensity features. Small scan line synchronization errors were corrected in these close-up images by shifting every other scan line by a single pixel (left for low Z and right for high Z) and scan line 126 was shifted 14 pixels to the right in the low-Z elements due to a small stepper motor malfunction at the start of this line. Fig. 5 and Fig. S3 followed a nearly identical preparation methodology; however, no synchronization corrections were needed in those cases. The iron map in Fig. 5 is simply a zoomed portion of the TIFF file with no additional processing. Pixel counts for the different anatomical regions are in Table S1.

The reason they are different is that we imaged a much larger part of the slab for the low-Z elements—however, they are all fairly large values—even for the teeth: ~690 samples means that the standard errors are all fairly small.

Sediment Analysis. A small ~0.2 g sample of sediment was taken from the reverse side of the specimen. Part of the solid was analyzed via X-ray diffraction with an internal Si standard and was clearly matched by a calcite reference pattern with no other phases determined. A second portion (0.101 g) was digested in 2% HCl to a final volume of 100 mL. Splits were taken and analyzed via inductively coupled plasma–mass spectrometry for Mn, Fe, Cu, Zn, and Pb and via inductively coupled plasma–atomic emission spectrometry for P and S. Concentrations given in Table 1 were blank corrected and recalculated to ppmw in the original solids. Excellent agreement with the X-ray analyses for all elements except S was achieved.

Probable Treatment History. Only a single slab exists for this fossil, with the counterpart unknown. The main slab of *Archaeopteryx* specimens should consist of the upper ("Hangendplatte") slab (7), as is the case with the Thermopolis specimen. This indicates that the Thermopolis specimen was preserved in a dorsal-side-up position (8, 9).

Maps show small (1 to 2 mm) areas of restoration on several of the larger bones (absence of P; see also Br map in Fig. S1). The left distal femur and the proximal tibia as well as the distal two-thirds of the right humerus have indeed been completely restored consistent with previous findings (9). The left leg and right arm were either damaged during preparation as the bones were uncovered or, more likely, these elements were split through natural causes as the matrix enclosing the fossil split along natural bedding planes. We also note that the distal right pes is not present. This portion of the fossil originally lay on the other side of a natural vertical fracture and was probably missed by the collector. Rock has clearly been added to replace the missing matrix in order to center the specimen. The XRF iron image (Fig. S1) reveals that this rock originated from the reverse side of the specimen and was affixed via polyester resin. The areas of restoration on the Thermopolis *Archaeopteryx* are typical for fossils prepared for exhibit. Revealed bone restoration and matrix transfer were probably undertaken solely for the purpose of aesthetics.

1. Popescu BFG, et al. (2009) Mapping metals in Parkinson's and normal brain using rapid-scanning x-ray fluorescence. *Phys Med Biol* 54:651–663.
2. Solé VA, Papillon E, Cotte M, Walter Ph, Susini J (2007) A multiplatform code for the analysis of energy-dispersive x-ray fluorescence spectra. *Spectrochim Acta Part B* 62:63–68.
3. Fedak TJ (2006) Using capillarity for determining and maintaining a polymer consolidant concentration after solution preparation. *Collection Forum* 20:108–112.
4. Pouli P, et al. (2009) Laser assisted removal of synthetic painting-conservation materials using UV radiation of ns and fs pulse duration: Morphological studies on model samples. *Appl Surf Sci* 255:4955–4960.
5. Photoshop CS3 Extended (version 10.0.1).
6. Dr. Keith Knox Boeing LTS, Chief Scientist Air Force Maui Optical & Supercomputing Site.
7. Elzanowski A (2002) Archaeopterygidae (Upper Jurassic of Germany). *Mesozoic Birds: Above the Heads of Dinosaurs*, eds Chiappe L, Witmer L (University of California Press, Berkeley), pp 129–159.
8. Mayr G, Pohl B, Peters DS (2005) A well-preserved *Archaeopteryx* specimen with theropod features. *Science* 310:1483–1486.
9. Mayr G, Pohl B, Hartman S, Peters DS (2007) The tenth skeletal specimen of *Archaeopteryx*. *Zool J Linn Soc-Lond* 149:97–116.

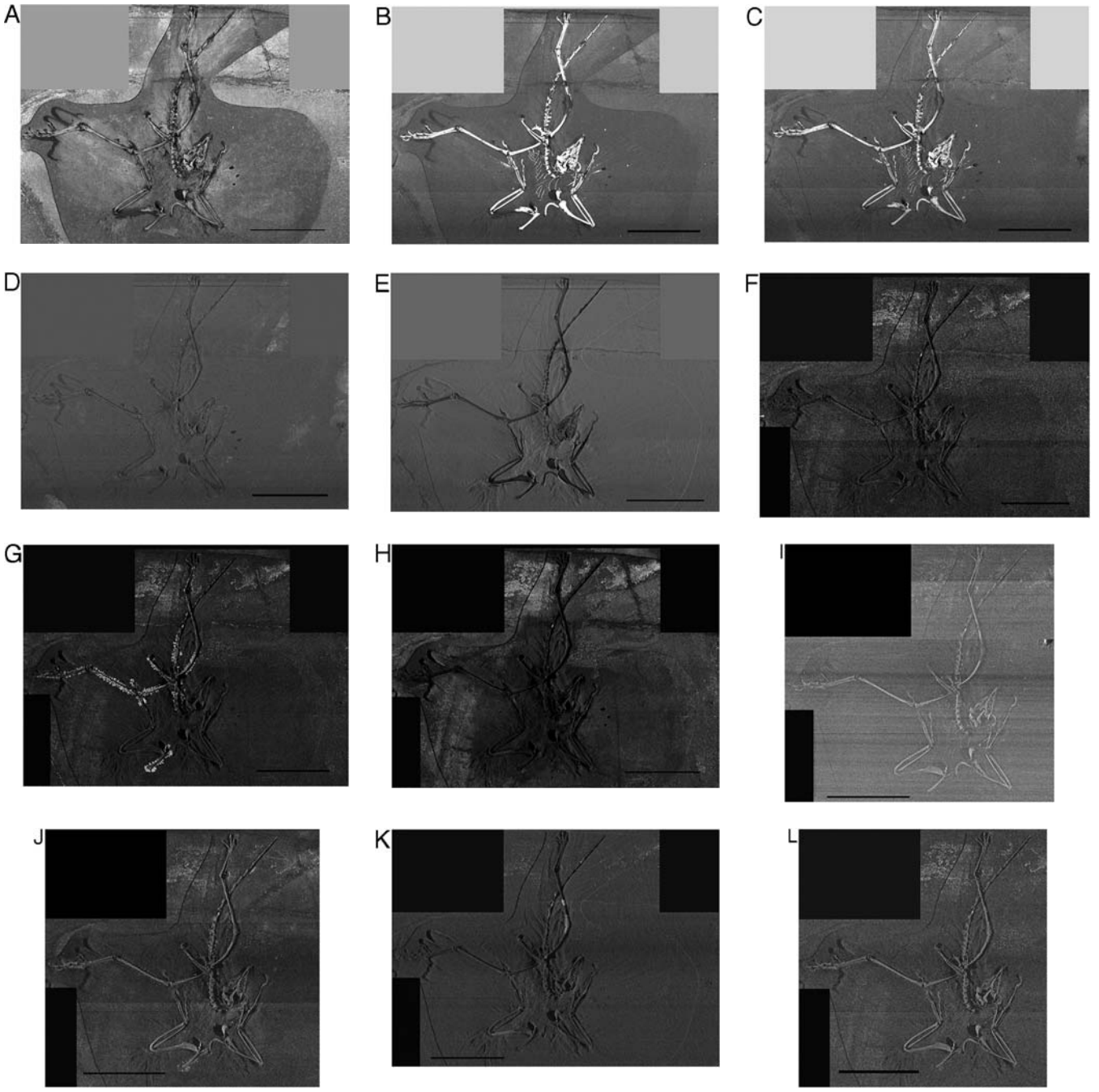

Fig. S1. (*A*) Si Kα. Si is present both in the sediment and associated with the fossil. All elemental maps in Fig. S1 are grayscale intensity maps with range determined by the dynamic range of counts in the detector for a given element. High concentrations correspond to white; low concentrations correspond to black. Topography contributes to some of the observed intensity fluctuations. (Scale bar, 10 cm.) (*B*) P Kα. Rachises and restored areas of bone are obvious. (Scale bar, 10 cm.) (*C*) S Kα. Distribution is similar to phosphorous except sulfur is not as concentrated in the rachises. (Scale bar, 10 cm.) (*D*) Cl Kα. Note the numerous fingerprints towards the edges of the specimen. (Scale bar, 10 cm.) (*E*) Ca Kα. Matrix of calcite is slightly higher in Ca than the bone apatite by approximately 1% by weight. (Scale bar, 10 cm.) (*F*) Ba Lα/ Ti Kα. This map is a convolution of the two signals. Attempts were made to avoid this overlap by narrowing the energy window, but the intensity was so low the window had to be left fairly wide. Point analyses indicated the presence of both Ti and Ba but concentrations were so low that they could not be reliably quantified or discriminated. (Scale bar, 10 cm.) (*G*) Mn Kα. Note the fine-scale dendritic precipitates of inorganic manganese oxide most likely formed by geochemical fluids long after deposition and controlled by the enhanced permeability created by the presence of the bone. Mn oxides also preferentially form along fractures in the Solenhofen limestone. (Scale bar, 10 cm.) (*H*) Fe Kα. Small iron oxyhydroxide precipitates dot the bedding plane interface. Some areas are quite high in Fe. (Scale bar, 10 cm.) (*I*) Zn Kα. Concentration levels are low with low contrast, but the measured factor of 2 difference between sediment and bone is clearly visible. (Scale bar, 10 cm.) (*J*) Cu Kα. Concentration levels are low with even lower contrast between bone and matrix than for Zn. (Scale bar, 10 cm.) (*K*) Br Kα. Anomalously high Br levels are clearly associated with the bone "filler" added by an unknown curator. (Scale bar, 10 cm.) (*L*) Pb Lα. Concentrations levels are lower than Cu or Zn in all point analyses; however, some of the iron oxyhydroxides in the upper portion of the scanned region show locally high Pb contents. (Scale bar, 10 cm.)

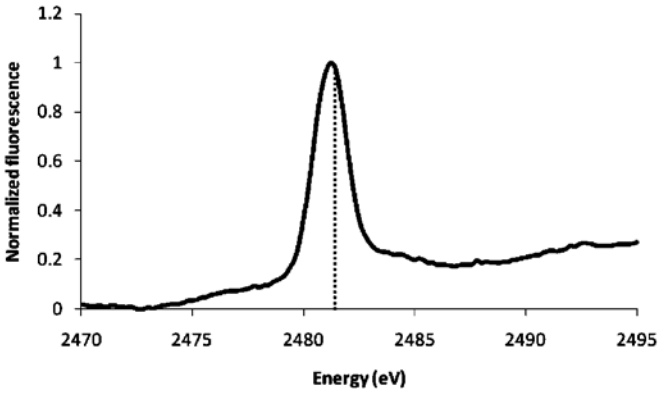

Fig. S2. Sulfur K-edge X-ray absorption near edge structure spectra from the humerus of the Thermopolis *Archaeopteryx* (*Solid Line*, maximum at 2481.2 eV) compared to the position of the absorption edge determined for a K_2SO_4 standard (*Vertical Dashed Line* at 2481.4 eV). The position of the peak in the *Archaeopteryx* spectrum indicates that the sulfur in the bone is dominantly present as sulfate. A low energy shoulder between 2475 and 2478 eV may indicate a small quantity of slightly reduced organic sulfur is present (sulfur-bearing compounds possible in this interval and their peak position relative to sulfate include: methsulfone, −3.6 eV; benzene-Σ, −2.2 eV; taurine, −1.6 eV; and SDS, −0.6 eV). In contrast, the presence of reduced species such as pyrite, sulfide, and disulfide are not consistent with this spectrum, indicating that the fossil has not been altered under conditions favoring replacement by pyrite.

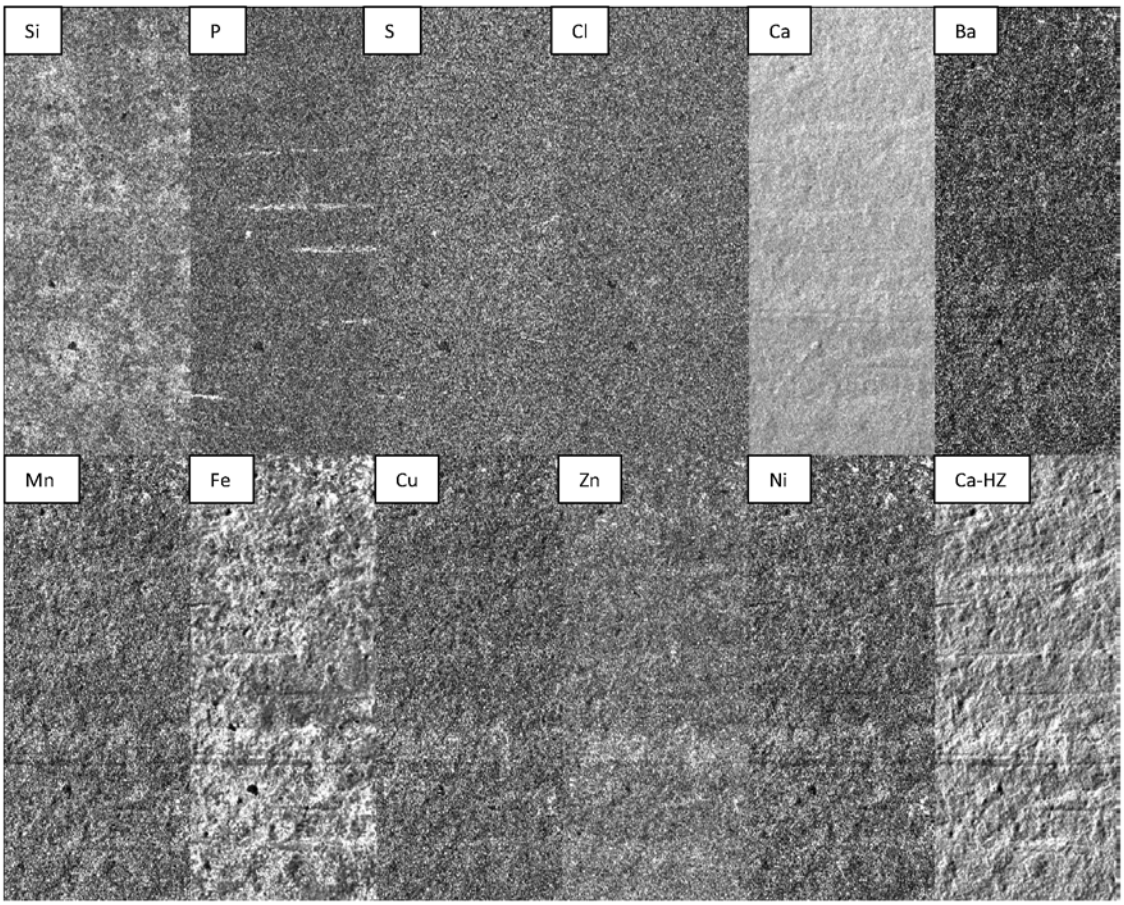

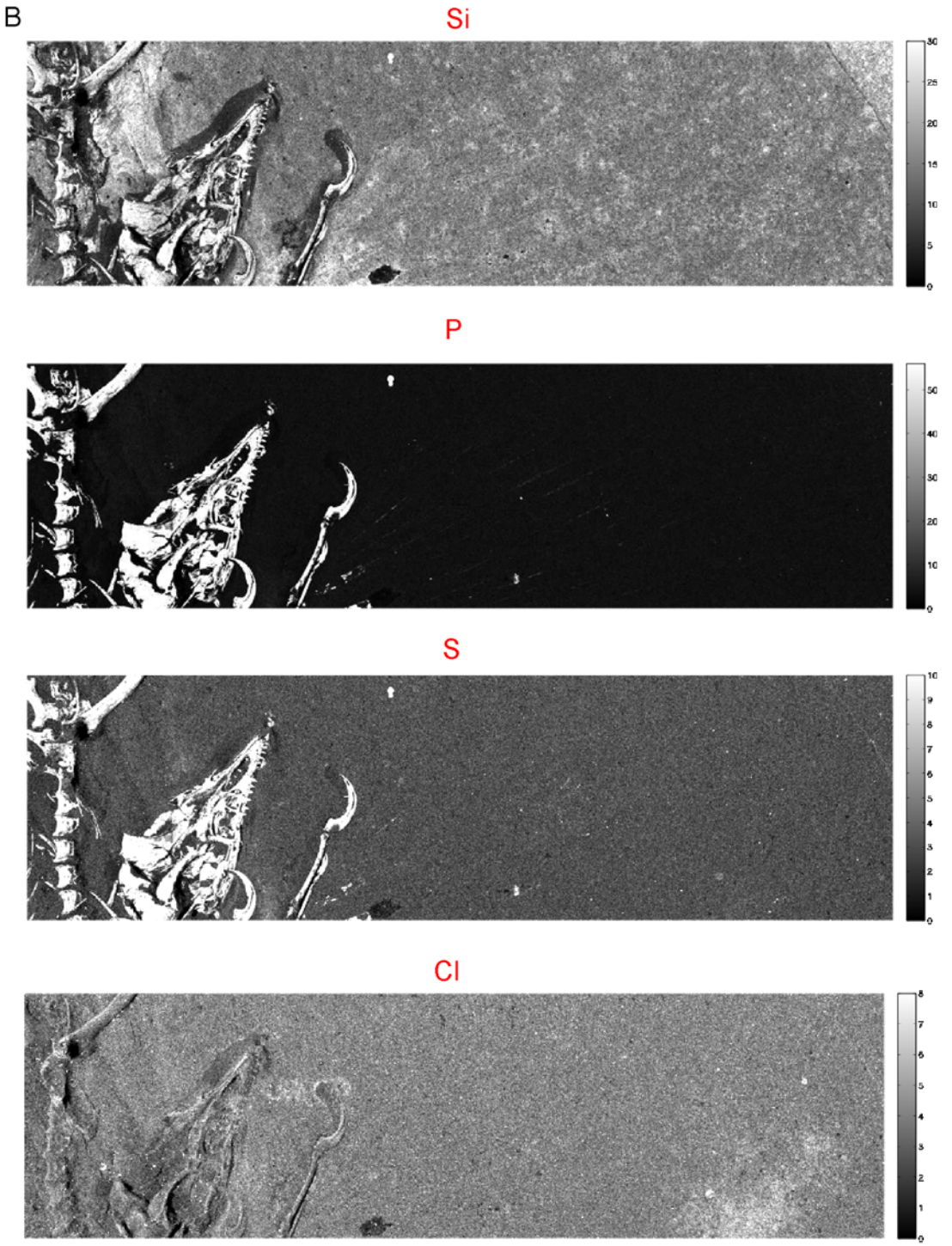
B
Si
P
S
Cl

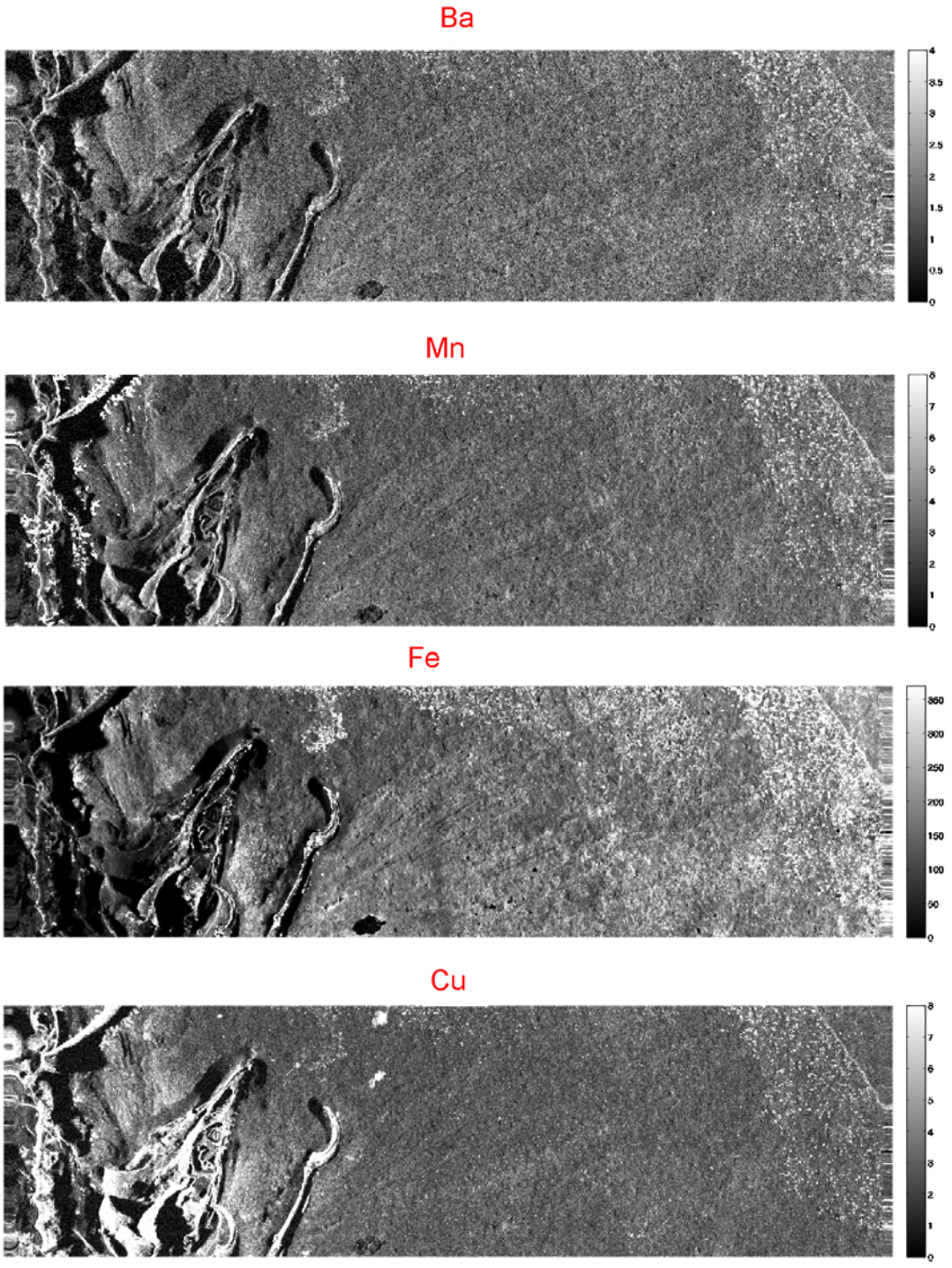
Ba
4
3.5
3
2.5
2
1.5
1
0.5
0
Mn
8
7
6
5
4
3
2
1
0
Fe
350
300
250
200
150
100
50
0
Cu
8
7
6
5
4
3
2
1
0

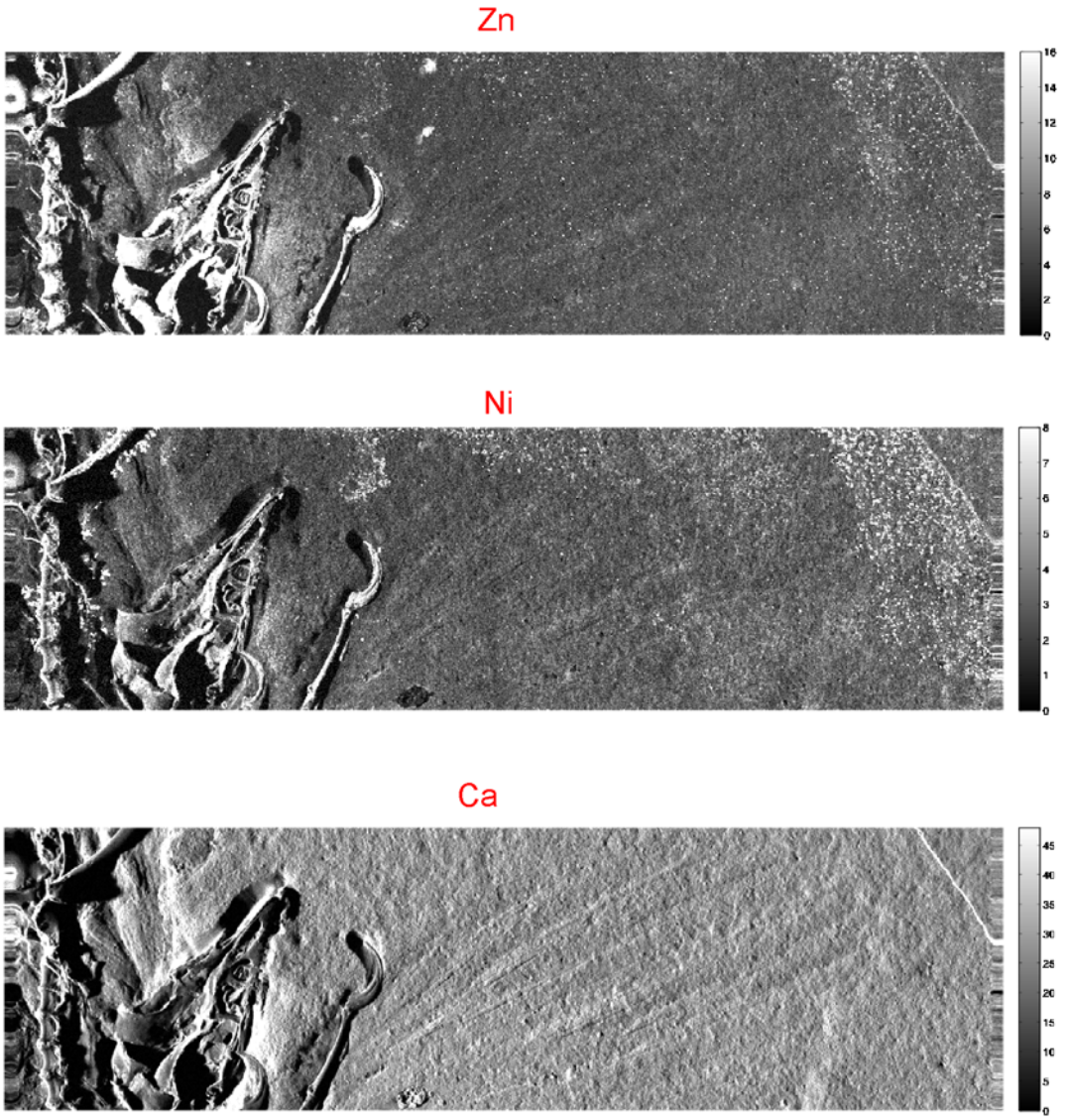

Fig. S3. (*A*) Detector count maps for all elements of the feather region clipped so that white corresponds to the 95th percentile of the overall count distribution. Two calcium maps are shown, one measured in low-Z configuration and one in high-Z configuration as discussed in the text. (*B*) Full set of elemental images corresponding to region presented in Fig. 2 with intensity scale included at right.

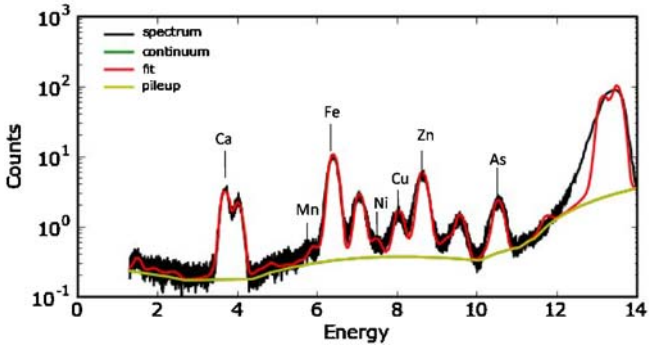

Fig. S4. Energy dispersive XRF point analysis spectrum taken from the *Archaeopteryx* skull at an incident energy of 13.5 keV. Fit corresponds to the quantitative result presented in Table 1 and was calculated using fundamental parameters as recorded during measurement; no normalization has been performed. Excellent agreement between the data and fit are achieved using PyMCA (2). Kα line positions are labeled.

Table S1. Numbers of pixels used for each region in anatomical correlate analysis

	High-Z pixel counts	Low-Z pixel counts
Bone	86,123	246,428
Claws	7,108	22,851
Feathers	1,289,332	1,345,347
Skull	89,044	111,472
Teeth	696	689
Slab	2,886,225	6,573,000